Int. J. Heat Mass Transfer. Vol. 27, No. 8, pp. 1345–1356, 1984
Printed in Great Britain

0017–9310/84 $3.00 + 0.00

FORCED CONVECTION HEAT AND MOMENTUM TRANSFER TO DENDRITIC STRUCTURES (PARABOLIC CYLINDERS AND PARABOLOIDS OF REVOLUTION)

SACHINDRA KUMAR DASH
Chemical Engineering Department, Iowa State University, Ames, IA 50011, U.S.A.

and

WILLIAM N. GILL*
Chemical Engineering Department, State University of New York at Buffalo, Amherst, NY 14260, U.S.A.

(*Received* 9 *May* 1983 *and in revised form* 14 *November* 1983)

Abstract—Three fundamental theoretical flow models including Oseen type rectilinear flow, potential flow, and Oseen's viscous flow approximation, are developed for forced convection heat transfer to parabolic cylinders and paraboloids of revolution which are relevant to dendritic growth. Closed-form results are obtained and presented in terms of Nusselt numbers at the stagnation point which are related to downstream values by analytical expressions. The heat flux from paraboloids of revolution is much larger than that for parabolic cylinders, especially at smaller values of the Peclet number. Local expressions for the heat flux are consistent with the shape preserving growth of these configurations as isothermal dendrites in forced convection fields. Diffusion of momentum and energy extends to significantly greater distances into the flow for parabolic cylinders than paraboloids of revolution. Boundary-layer assumptions would lead to large errors for the conditions studied here, especially for low *Pr* fluids. The results are useful for describing the diffusion of mass also.

NOMENCLATURE

$\mathbf{e}$	unit vectors
h	heat transfer coefficient
k	thermal conductivity
n	normal to the interface
Nu	Nusselt number, hR/k
p	pressure
Pe	Peclet number, $U_\infty R/\alpha$
Pr	Prandtl number, ν/α
R	tip radius
Re	Reynolds number, $U_\infty R/\nu$
t	temperature
u, v, w	velocity components
U_∞	freestream velocity
x, y, z	coordinate axes
X, Y, Z	reduced coordinate axes.

Greek symbols

α	thermal diffusivity of the liquid
θ	dimensionless temperature
ν	viscosity of the liquid
ξ, η, ϕ	parabolic coordinate axes
ρ	density of the liquid.

Superscipts

	perturbed velocity.

Subscripts

p	potential flow
w	wall or interface
∞	far from the body
x, y, z, ξ, η, ϕ	directions.

INTRODUCTION

DENDRITES are reported to grow as platelets and needles for which the best approximations of the shape are parabolic cylinders and paraboloids of revolution, respectively. In many cases, dendrites grow by transferring the latent heat from their interfaces to the undercooled melt. Thus, by calculating the heat transfer rate from the interface of the dendrite one can predict its growth rate providing the growth rate is controlled by heat transfer to the melt. Sometimes growth rates are affected also by kinetic and/or mass transfer effects especially when the melt is a solution (a mixture) from which only one component is incorporated into the growing crystal, e.g. ice growth from salt water.

The first successful attempt to predict theoretically the heat transfer rate from needle-shaped crystals was made by Ivantsov [1]. He proved that a steady-state solution exists for a needle-shaped isothermal crystal growing in a shape preserving manner in an undercooled melt where molecular diffusion is the only mode of heat transfer. Horvay and Cahn [2] extended Ivantsov's result to parabolic cylinders and elliptic paraboloids. However, dendritic growth rarely occurs without an accompanying fluid flow. In the

* To whom correspondence should be directed.

cooled melt flow patterns may occur due to gravity or by forced convection mechanisms.

Very few forced or natural convection heat transfer results exist for parabolic cylinders and paraboloids of revolution. Huang [3], made boundary layer calculations, in which conduction along streamlines was neglected, for natural convection heat transfer from the stagnation region of a parabolic cylinder. Squire [4] has given a method for calculating the forced convection heat transfer from the stagnation region of any cylinder, and other articles, for example Frossling [5], are available which also include boundary-layer theory calculations for forced convection heat transfer from cylinders and bodies of revolution, but this work is not applicable to low Peclet number flows.

Crystal growth phenomena under forced convection conditions have been studied experimentally by Barduhn *et al.* (see refs. [3, 6–10]), Simpson *et al.* [11, 12] and Fujioka [13] who observed ice crystals to grow as elliptic paraboloids with an aspect ratio of 70–100 for which a good approximation is a parabolic cylinder with a tip radius of the order of 1–10 μm. Due to the small dimension of the crystals, the Reynolds and Peclet numbers are very low and for such situations no forced convection heat transfer analyses exist in the literature which include conduction along streamlines. The purpose of this paper is to develop some useful heat transfer results for low Reynolds number flows over parabolic cylinders and paraboloids of revolution. These results are calculated from the new solutions which are developed here for the three flow fields given below:

(1) Oseen type rectilinear flow approximation (ORFA);

(2) Oseen's viscous flow approximation (OVFA);

(3) potential flow approximation.

It is shown that closed-form exact solutions exist which satisfy the partial differential energy equations (26), (34), (76), (78), (87) and (88), which apply to all three flow fields and both configurations, and which also satisfy all four boundary conditions given in equations (27), (35) or (77) for all six cases at $\eta = 0$ and $\eta \to \infty$ as well as $\xi = 0$ and $\xi \to \infty$. Therefore, these solutions which are functions of η only, are valid throughout the entire domain of both ξ and η.

It should be noted that one obviously can use the present results to calculate dendritic growth rates and tip radii in the same way as boundary-layer results have been used by Fernandez and Barduhn [6] wherein the maximum growth principle was employed. The application of the present results and others which we have developed to predict dendrite behavior is a separate topic that is now under active consideration in our laboratory from both maximum growth and stability viewpoints.

THEORY

The ORFA was used initially by Cole and Roshko [14] for a circular cylinder. The flow field is assumed to be constant and such that the fluid does not react to the body at all. This assumption is good for very low Reynolds number flows of low Prandtl number fluids. Moreover, if the Reynolds number is small due to the small characteristic dimension of the body, this implies that most of the fluid will be moving at the undisturbed freestream velocity, U_∞, and if the Prandtl number is small most of the resistance to heat transfer lies in the undisturbed fluid stream.

The differential equation for heat transfer with Oseen type rectilinear flow is given by

$$\mathbf{U}_\infty \cdot \nabla t = \alpha \nabla^2 t, \tag{1}$$

and the boundary conditions are

$$\begin{aligned} t &= t_w \quad \text{on the body,} \\ t &= t_\infty \quad \text{far from the body.} \end{aligned} \tag{2}$$

The approximation that $\mathbf{u} = \mathbf{U}_\infty$ seems to give fairly good results for heat transfer from circular cylinders to air ($Pr = 0.7$) at low Reynolds number ($\ll 1$) as shown by Cole and Roshko [14] and their result is exactly the first-order term of the matched asymptotic expansion solution of Hieber and Gebhart [15] for the Nusselt number for a circular cylinder at low Reynolds and Peclet numbers. Their second-order term was negative and rather small. Thus, Cole and Roshko's result gives a reasonably accurate and simple approximate solution.

Since all real fluids have finite viscosity, OVFA, which is valid for low Reynolds number flows, was determined. It includes viscous and first-order acceleration effects. The result presented here is valid for all Prandtl numbers. First, the flow field is determined with Oseen's approximation and then the velocity field thus obtained is used to solve for the heat transfer results. The validity of the results obtained depends on how accurately the flow field is represented by Oseen's approximation.

Comparison of the results obtained by using the OVFA to calculate the skin friction with Davis and Werle's [16] numerical solution for a paraboloid of revolution shows that they agree fairly well up to $Re = 1.0$.

With OVFA the differential equation and boundary conditions for any geometry are given by

$$\nabla \cdot \mathbf{u} = 0 \quad \text{(continuity)}, \tag{3a}$$

$$\mathbf{U}_\infty \cdot \nabla \mathbf{u} = -\frac{1}{\rho} \nabla p + \nu \nabla^2 \mathbf{u} \quad \text{(momentum transfer)}, \tag{3b}$$

$$\mathbf{u} \cdot \nabla t = \alpha \nabla^2 t, \quad \text{(energy)} \tag{4}$$

$$\begin{aligned} \mathbf{u} &= 0, \quad t = t_w \quad \text{on the body,} \\ \mathbf{u} &= \mathbf{U}_\infty, \quad t = t_\infty \quad \text{far from the body.} \end{aligned} \tag{5}$$

The flow field was solved first by Wilkinson [17] for both parabolic cylinders and paraboloids of revolution. However, he presented only the method of solution. He did not give the expression for the velocity explicitly. In the present work, the results are provided in a more complete form.

The potential flow approximation is valid for high Reynolds number flows of low Prandtl number fluids like liquid metals in which dendritic growth is of great practical importance. For these cases, the thermal boundary layer is much thicker than the momentum boundary layer, and outside the momentum boundary layer, potential flow exists. Hence, most of the resistance to heat transfer lies in the region where the flow field closely approximates potential flow.

With the potential flow assumptions, the governing differential equation and the boundary conditions for any geometry are

$$\mathbf{u}_p \cdot \nabla t = \alpha \nabla^2 t, \tag{6}$$

$$\begin{aligned} t &= t_w \quad \text{on the body,} \\ t &= t_\infty \quad \text{far from the body,} \end{aligned} \tag{7}$$

where $\mathbf{u}_p$ is the potential flow velocity.

Figures 1(a) and (b) show the configurations considered here.

Because the body is of the form of a parabolic cylinder (two-dimensional) or a paraboloid of revolution (three-dimensional), it is convenient to use parabolic coordinates which is an orthogonal curvilinear coordinate system.

Parabolic cylinders [Fig.1(a)]

For the parabolic cylinder, the following transformations are made

$$\begin{aligned} \frac{x}{R} &= X = (\xi^2 - \eta^2)/2, \\ \frac{z}{R} &= Z = \xi\eta, \\ \frac{y}{R} &= Y = Y. \end{aligned} \tag{8}$$

Under the transformation of equation (8), the surface of the body is represented as $\eta = 1, -1$ and the domain outside the body is given by $0 \leqslant \xi \leqslant \infty$, $-\infty \leqslant \eta \leqslant \infty$, excluding $-1 \leqslant \eta \leqslant 1$, and $-\infty \leqslant Y \leqslant \infty$.

The relations between unit vectors in Cartesian coordinates to those in parabolic coordinates for a parabolic cylinder are given by

$$\mathbf{e}_x = \frac{\xi}{\sqrt{(\xi^2+\eta^2)}}\mathbf{e}_\xi - \frac{\eta}{\sqrt{(\xi^2+\eta^2)}}\mathbf{e}_\eta, \tag{9}$$

$$\mathbf{e}_z = \frac{\eta}{\sqrt{(\xi^2+\eta^2)}}\mathbf{e}_\xi + \frac{\xi}{\sqrt{(\xi^2+\eta^2)}}\mathbf{e}_\eta. \tag{10}$$

The scale factors are given by

$$h_\xi = h_\eta = R\sqrt{(\xi^2+\eta^2)}, \tag{11}$$

$$h_y = R. \tag{12}$$

The heat equation is given by

$$u_\xi \frac{1}{\sqrt{(\xi^2+\eta^2)}}\frac{\partial t}{\partial \xi} + u_\eta \frac{1}{\sqrt{(\xi^2+\eta^2)}}\frac{\partial t}{\partial \eta} + u_y \frac{\partial t}{\partial Y} = \frac{\alpha}{R(\xi^2+\eta^2)}\left[\frac{\partial^2 t}{\partial \xi^2} + \frac{\partial^2 t}{\partial \eta^2}\right] + \frac{\alpha}{R}\frac{\partial^2 t}{\partial Y^2}. \tag{13}$$

If t is not a function of Y, then the Y-derivative terms drop out.

The x-derivative, which is to be used explicitly, is given by

$$\frac{\partial}{\partial X} = \frac{\xi}{\xi^2+\eta^2}\frac{\partial}{\partial \xi} - \frac{\eta}{(\xi^2+\eta^2)}\frac{\partial}{\partial \eta}. \tag{14}$$

Paraboloid of revolution [Fig. 1(b)]

The equations for the three-dimensional transformation needed for a paraboloid of revolution are

$$\begin{aligned} x/R &= X = (\xi^2 - \eta^2)/2, \\ y/R &= Y = \xi\eta \sin\phi, \\ z/R &= Z = \xi\eta \cos\phi. \end{aligned} \tag{15}$$

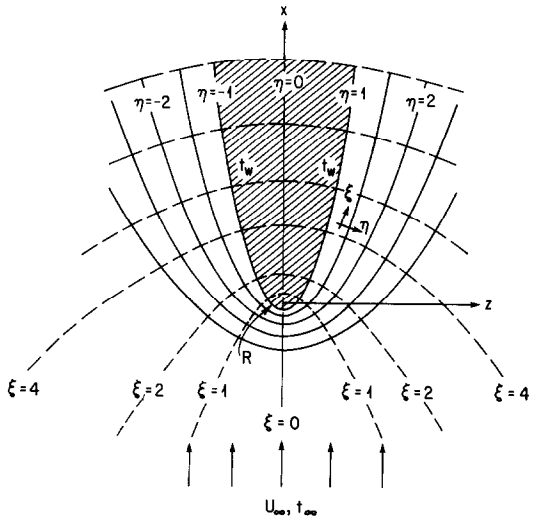

FIG. 1(a). Forced convection heat transfer from parabolic cylinders. The surface of the parabolic cylinder is represented by $\eta = 1$ and -1.

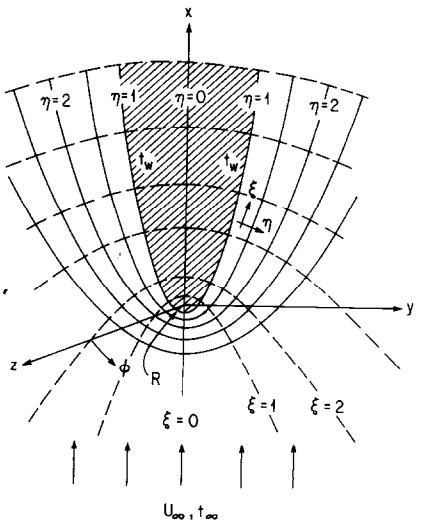

FIG. 1(b). Forced convection heat transfer from paraboloids of revolution. The surface of the paraboloid of revolution is represented by $\eta = 1$.

Under these transformations, the surface of the body is given by $\eta = 1$, and the whole domain outside the body is given by $1 \leqslant \eta \leqslant \infty, 0 \leqslant \xi \leqslant \infty, 0 \leqslant \phi \leqslant 2\pi$.

The relations between unit vectors in Cartesian coordinates and those in parabolic coordinates are given for a paraboloid of revolution by

$$\mathbf{e}_x = \frac{\xi}{\sqrt{(\xi^2+\eta^2)}}\mathbf{e}_\xi - \frac{\eta}{\sqrt{(\xi^2+\eta^2)}}\mathbf{e}_\eta, \tag{16}$$

$$\mathbf{e}_y = \frac{\eta \sin\phi}{\sqrt{(\xi^2+\eta^2)}}\mathbf{e}_\xi + \frac{\xi \sin\phi}{\sqrt{(\xi^2+\eta^2)}}\mathbf{e}_\eta - \cos\phi\mathbf{e}_\phi, \tag{17}$$

$$\mathbf{e}_z = \frac{\eta \cos\phi}{\sqrt{(\xi^2+\eta^2)}}\mathbf{e}_\xi + \frac{\xi \cos\phi}{\sqrt{(\xi^2+\eta^2)}}\mathbf{e}_\eta + \sin\phi\mathbf{e}_\phi. \tag{18}$$

The scale factors are given by

$$h_\xi = h_\eta = R\sqrt{(\xi^2+\eta^2)}, \tag{19}$$

$$h_\phi = R\xi\eta. \tag{20}$$

The convection equation is given by

$$u_\xi \frac{1}{\sqrt{(\xi^2+\eta^2)}}\frac{\partial t}{\partial \xi} + u_\eta \frac{1}{\sqrt{(\xi^2+\eta^2)}}\frac{\partial t}{\partial \eta} + \frac{u_\phi}{\xi\eta}\frac{\partial t}{\partial \phi} = \frac{\alpha}{R}\left[\frac{1}{(\xi^2+\eta^2)}\left\{\frac{\partial^2 t}{\partial \xi^2} + \frac{1}{\xi}\frac{\partial t}{\partial \xi} + \frac{\partial^2 t}{\partial \eta^2} + \frac{1}{\eta}\frac{\partial t}{\partial \eta}\right\} + \frac{1}{\xi^2\eta^2}\frac{\partial^2 t}{\partial \phi^2}\right]. \tag{21}$$

The ϕ dependent terms drop out due to symmetry.

The x-derivative, which is used explicitly is given by

$$\frac{\partial}{\partial X} = \frac{\xi}{(\xi^2+\eta^2)}\frac{\partial}{\partial \xi} - \frac{\eta}{(\xi^2+\eta^2)}\frac{\partial}{\partial \eta}. \tag{22}$$

ANALYSIS, RESULTS AND DISCUSSION

For both configurations the body is stationary, and is represented by $\eta = 1$, and the fluid flow is in the x-direction such that the tip of the parabola is the stagnation point. The body surface is at the temperature t_w and the freestream is at t_∞. Heat transfer occurs from the body to the fluid in dendritic growth in subcooled melts.

Oseen type rectilinear flow approximation (ORFA)

Parabolic cylinder. For the configuration given in Fig. 1(a), equation (1) and the boundary conditions [equation (2)] can be written as

$$\frac{\partial^2\theta}{\partial X^2} + \frac{\partial^2\theta}{\partial Z^2} - Pe\frac{\partial\theta}{\partial X} = 0, \tag{23}$$

where

$$X = x/R, \quad Z = z/R, \quad Pe = \frac{U_\infty R}{\alpha}, \tag{24}$$

and

$$\begin{aligned} &\theta = 1 \quad \text{on the body, i.e. at } X = \frac{Z^2-1}{2}, \\ &\theta = 0 \quad \text{far from the body.} \end{aligned} \tag{25}$$

Equations (23) and (25) can be changed to parabolic coordinates with the help of equations (8)–(14)

$$\left[\frac{\partial^2\theta}{\partial\xi^2} + \frac{\partial^2\theta}{\partial\eta^2}\right] - Pe\left[\xi\frac{\partial\theta}{\partial\eta} - \eta\frac{\partial\theta}{\partial\eta}\right] = 0, \tag{26}$$

and the boundary conditions become:

$$\begin{aligned} &\text{at } \eta = 1;\ \theta = 1 \quad \text{body temperature,} \\ &\text{at } \eta \to \infty;\ \theta \to 0 \quad \text{freestream temperature,} \\ &\text{at } \xi = 0;\ \frac{\partial\theta}{\partial\xi} = 0 \quad \text{due to symmetry,} \\ &\text{as } \xi \to \infty;\ \theta \quad \text{is finite.} \end{aligned} \tag{27}$$

The solution to equation (26) which satisfies equation (27) is given by

$$\theta = \frac{t-t_\infty}{t_w-t_\infty} = \frac{\operatorname{erfc}\{\sqrt{(Pe/2)}\eta\}}{\operatorname{erfc}\{\sqrt{(Pe/2)}\}}. \tag{28}$$

Defining the heat transfer coefficient by the ratio of the total heat flux to the temperature difference, one obtains

$$h(t_w-t_\infty) = -k\left.\frac{\partial t}{\partial n}\right|_{\eta=1} + \rho U_n C_p(t_w-t_\infty)\Big|_{\eta=1}, \tag{29}$$

where $\partial t/\partial n|_{\eta=1}$ is the normal temperature gradient at the interface of the body, and U_n is the component of velocity vector $\mathbf{U}_\infty$ normal to the interface of the body.

In equation (29), the first term on the RHS is the diffusive heat flux from the body and the second term is the convective heat flux. The convective term arises because the fluid passes right through the body. U_n can be estimated by taking the dot product of $U_\infty\mathbf{e}_x$ with $\mathbf{e}_\eta$. Equation (9) is useful in obtaining the expression for U_n. Using equations (9) and (28) in equation (29), one obtains

$$h(t_w-t_\infty) = -k(t_w-t_\infty)\frac{1}{R}\frac{1}{\sqrt{(\xi^2+\eta^2)}}\left.\frac{\partial\theta}{\partial\eta}\right|_{\eta=1} - \rho\left.\frac{U_\infty\eta}{\sqrt{(\xi^2+\eta^2)}}\right|_{\eta=1}^{C_p(t_w-t_\infty)}.$$

Hence

$$Nu(\xi) = \frac{hR}{k} = \frac{1}{\sqrt{(1+\xi^2)}} \times \left[\sqrt{\left(\frac{2Pe}{\pi}\right)}\frac{e^{-Pe/2}}{\operatorname{erfc}\{\sqrt{(Pe/2)}\}} - Pe\right], \tag{30}$$

where $Pe = U_\infty R/\alpha$. If the heat transfer coefficient in equation (30) had been defined in terms of only the diffusive contribution at the interface, then the last term in equation (30), $-Pe$, would not appear.

The ORFA is valid for low Reynolds and Prandtl number flows which implies the Peclet number (Pe) is low, and one can neglect the second term in the brackets on the RHS of equation (30). For example, for $Pe = 0.01$

$$\sqrt{\left(\frac{2Pe}{\pi}\right)}\frac{e^{-Pe/2}}{\operatorname{erfc}\{\sqrt{(Pe/2)}\}} = 0.085,$$

which is much bigger than Pe. So for low Peclet numbers, equation (30) becomes

$$Nu = \frac{hR}{k} = (1+\xi^2)^{-1/2}\sqrt{\left(\frac{2Pe}{\pi}\right)}\frac{e^{-Pe/2}}{\text{erfc}\{\sqrt{(Pe/2)}\}}. \quad (31)$$

At the stagnation point ($\xi = 0$) equation (31) gives

$$Nu = \frac{hR}{k} = \sqrt{\left(\frac{2Pe}{\pi}\right)}\frac{e^{-Pe/2}}{\text{erfc}\{\sqrt{(Pe/2)}\}}. \quad (32)$$

Although the physical situation with OFRA is totally different, the mathematical solution is seen here to be identical to that for pure conduction with a moving boundary as solved by Horvay and Cahn [2].

Paraboloid of revolution. For the configuration given in Fig. 1(b), equation (1) and the boundary conditions, equation (2), become

$$U_\infty \frac{\partial t}{\partial x} = \alpha\left(\frac{\partial^2 t}{\partial x^2} + \frac{\partial^2 t}{\partial y^2} + \frac{\partial^2 t}{\partial z^2}\right), \quad (33)$$

$$t = t_w \quad \text{on the body, i.e. at } \frac{x}{R} = \frac{[(y^2+z^2)/R^2]-1}{2},$$

and

$$t = t_\infty \quad \text{far from the body.}$$

Changing to parabolic coordinates by use of equations (15)–(22), making equation (33) dimensionless, and neglecting $\partial/\partial\phi$ terms due to symmetry, one obtains

$$\frac{\partial^2\theta}{\partial\xi^2} + \left(\frac{1}{\xi} - Pe\ \xi\right)\frac{\partial\theta}{\partial\xi} + \frac{\partial^2\theta}{\partial\eta^2} + \left(\frac{1}{\eta} + Pe\ \eta\right)\frac{\partial\theta}{\partial\eta} = 0, \quad (34)$$

with

$$\begin{aligned} &\text{at } \eta = 1;\ \theta = 1,\\ &\text{as } \eta \to \infty;\ \theta \to 0,\\ &\text{at } \xi = 0;\ \frac{\partial\theta}{\partial\xi} = 0 \text{ (symmetry)},\\ &\text{as } \xi \to \infty;\ \theta \text{ is finite,} \end{aligned} \quad (35)$$

where $Pe = U_\infty R/\alpha$.

The solution of equations (34) and (35) is given by

$$\theta = \frac{t-t_\infty}{t_w-t_\infty} = \frac{E_1[(Pe/2)\eta^2]}{E_1[(Pe/2)]}, \quad (36)$$

where $E_1(x)$ is the exponential integral and is given by

$$E_1(x) = \int_x^\infty \frac{e^{-t}}{t}\,dt. \quad (37)$$

Defining the heat transfer coefficient by equation (29) and using equations (36) and (16) in equation (29), one obtains

$$Nu(\xi) = \frac{hR}{k} = \frac{1}{\sqrt{(1+\xi^2)}}\frac{2e^{-Pe/2}}{E_1(Pe/2)} - Pe. \quad (39)$$

At the stagnation point $\xi = 0$, the Nusselt number is given by

$$Nu = \frac{hR}{k} = \frac{2e^{-Pe/2}}{E_1(Pe/2)} - Pe. \quad (40)$$

Figure 2 compares the result given by equations (32) and (40), where $(-Pe)$ in equation (40) is dropped, and it shows the effect of shape on the heat transfer coefficient. One sees that the heat transfer coefficient for a paraboloid of revolution is much larger than that for a parabolic cylinder, especially at smaller values of Pe. The smaller differences at higher Peclet numbers occur because convection plays a more important role in heat transfer, and the convection field, as considered here, is unaffected by the presence of the body, this becomes clear if one substitutes $\partial\theta/\partial\xi = \partial^2\theta/\partial\xi^2 = 0$ in equations (26) and (34), and compares the resulting equations for high values of Pe when $1/\eta \ll Pe\ \eta$ because $\eta \geqslant 1$. Thus, one can neglect $1/\eta$ in equation (34) at high Pe and the resulting equations become identical and yield identical results. Equations (32) and (40) are more accurate at low Peclet numbers. However, in Fig. 2 the results are extrapolated up to a Peclet number of 1 for illustrative purposes.

Oseen's viscous flow approximation (OVFA)

Here Oseen's viscous flow approximation is applied to parabolic cylinders and paraboloids of revolution. First, it is necessary to solve for the velocity distributions because explicit expressions are not available. For these cases [shown in Figs. 1(a) and (b)] the differential equations and the boundary conditions [equations (3a) and (3b)] and equation (5) can be written as

$$\frac{\partial u}{\partial x} + \frac{\partial v}{\partial y} + \frac{\partial w}{\partial z} = 0, \quad (41)$$

$$U_\infty \frac{\partial u}{\partial x} = -\frac{1}{\rho}\frac{\partial p}{\partial x} + \nu\left(\frac{\partial^2 u}{\partial x^2} + \frac{\partial^2 u}{\partial y^2} + \frac{\partial^2 u}{\partial z^2}\right), \quad (42)$$

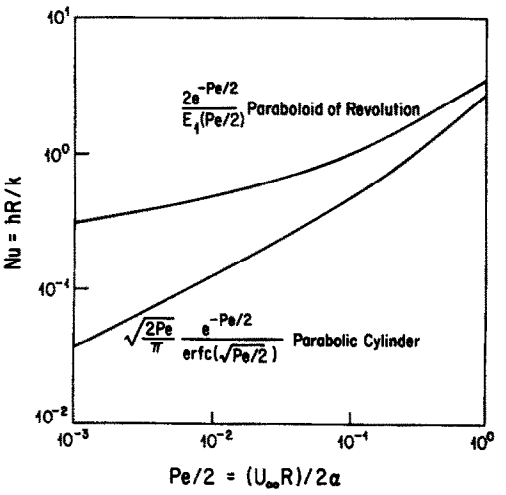

FIG. 2. Nusselt number at the stagnation point vs Peclet number of parabolic cylinders and paraboloids of revolution with ORFA.

$$U_\infty \frac{\partial v}{\partial x} = -\frac{1}{\rho}\frac{\partial p}{\partial y} + \nu\left(\frac{\partial^2 v}{\partial x^2} + \frac{\partial^2 v}{\partial y^2} + \frac{\partial^2 v}{\partial z^2}\right), \quad (43)$$

$$U_\infty \frac{\partial w}{\partial x} = -\frac{1}{\rho}\frac{\partial p}{\partial z} + \nu\left(\frac{\partial^2 w}{\partial x^2} + \frac{\partial^2 w}{\partial y^2} + \frac{\partial^2 w}{\partial z^2}\right). \quad (44)$$

Here, u, v and w are the components of the velocity vector $\mathbf{u}$ in the x-, y- and z-directions, respectively, and p is the pressure. The boundary conditions are

$$u = 0, \quad v = w, \quad 0 \text{ on the body}, \quad (45)$$

$$u = U_\infty, \quad v = w = 0 \quad \text{far from the body}. \quad (46)$$

Now if we let

$$\mathbf{u} = \mathbf{U}_\infty - \mathbf{u}', \quad (47)$$

where $\mathbf{u}'$ is the perturbed velocity vector whose components are u', v', and w' along x-, y- and z-directions, respectively, the boundary conditions become

$$u' = U_\infty, \quad v' = w' = 0 \quad \text{on the body}, \quad (48)$$

$$u' = v' = w' = 0 \quad \text{far from the body}, \quad (49)$$

and equations (41)–(44), after the transformation $X = x/R$, $Y = y/R$, $Z = z/R$, and $Re = U_\infty R/\nu$, are

$$\frac{\partial u'}{\partial X} + \frac{\partial v'}{\partial Y} + \frac{\partial w'}{\partial Z} = 0, \quad (50)$$

$$Re\frac{\partial u'}{\partial X} = -\frac{1}{\rho}\frac{R}{\nu}\frac{\partial p}{\partial X} + \left(\frac{\partial^2 u'}{\partial X^2} + \frac{\partial^2 u'}{\partial Y^2} + \frac{\partial^2 u'}{\partial Z^2}\right), \quad (51)$$

$$Re\frac{\partial v'}{\partial X} = -\frac{1}{\rho}\frac{R}{\nu}\frac{\partial p}{\partial Y} + \left(\frac{\partial^2 v'}{\partial X^2} + \frac{\partial^2 v'}{\partial Y^2} + \frac{\partial^2 v'}{\partial Z^2}\right), \quad (52)$$

$$Re\frac{\partial w'}{\partial X} = -\frac{1}{\rho}\frac{R}{\nu}\frac{\partial p}{\partial Z} + \left(\frac{\partial^2 w'}{\partial X^2} + \frac{\partial^2 w'}{\partial Y^2} + \frac{\partial^2 w'}{\partial Z^2}\right). \quad (53)$$

If M and N are defined such that

$$u' = \frac{\partial M}{\partial X} + \frac{1}{Re}\frac{\partial N}{\partial X} - N, \quad (54)$$

$$v' = \frac{\partial M}{\partial Y} + \frac{1}{Re}\frac{\partial N}{\partial Y}, \quad (55)$$

$$w' = \frac{\partial M}{\partial Z} + \frac{1}{Re}\frac{\partial N}{\partial Z}, \quad (56)$$

and

$$p = -\frac{\rho\nu}{R} Re\frac{\partial M}{\partial X}, \quad (57)$$

equations (50) and (53) are satisfied only if equations (58) and (59) are satisfied

$$\frac{\partial^2 M}{\partial X^2} + \frac{\partial^2 M}{\partial Y^2} + \frac{\partial^2 M}{\partial Z^2} = 0, \quad (58)$$

$$\frac{\partial^2 N}{\partial X^2} + \frac{\partial^2 N}{\partial Y^2} + \frac{\partial^2 N}{\partial Z^2} = Re\frac{\partial N}{\partial X}. \quad (59)$$

Hence, the solution to Oseen's viscous flow equation boils down to solving equations (58) and (59) with the boundary conditions of equations (48) and (49).

Equations (58) and (59) are transformed to parabolic cylinder and paraboloid of revolution coordinates by using equations (11)–(22). Here, the Y-component for the parabolic cylinder and the ϕ-component for the paraboloid of revolution vanish. The equations so obtained are given below:

For a parabolic cylinder, equations (58) and (59) become

$$\frac{\partial^2 M}{\partial \xi^2} + \frac{\partial^2 M}{\partial \eta^2} = 0, \quad (60)$$

$$\left(\frac{\partial^2 N}{\partial \xi^2} + \frac{\partial^2 N}{\partial \eta^2}\right) = Re\left\{\xi\frac{\partial N}{\partial \eta} - \eta\frac{\partial N}{\partial \eta}\right\}. \quad (61)$$

For a paraboloid of revolution they become

$$\frac{\partial^2 M}{\partial \xi^2} + \frac{1}{\xi}\frac{\partial M}{\partial \xi} + \frac{\partial^2 M}{\partial \eta^2} + \frac{1}{\eta}\frac{\partial M}{\partial \eta} = 0, \quad (62)$$

$$\frac{\partial^2 N}{\partial \xi^2} + \frac{1}{\xi}\frac{\partial N}{\partial \xi} + \frac{\partial^2 N}{\partial \eta^2} + \frac{1}{\eta}\frac{\partial N}{\partial \eta} = Re\left[\xi\frac{\partial N}{\partial \xi} - \eta\frac{\partial N}{\partial \eta}\right]. \quad (63)$$

The solutions of equations (60)–(63) are given below:

For the parabolic cylinder

$$M = A\eta + B, \quad (64)$$

$$N = C_1\int_0^\eta e^{-Ret^2/2}\,dt + C_2. \quad (65)$$

For the paraboloid of revolution

$$M = A\log\eta + B, \quad (66)$$

$$N = C_1\int_\eta^\infty \frac{e^{-Ret^2/2}}{t}\,dt + C_2, \quad (67)$$

where A, B, C_1 and C_2 are the constants of integration.

The expressions for M and N were substituted into equations (54)–(56). The resulting expressions were made to satisfy the boundary conditions, equation (48) at $\eta = 1$ and equation (49) at $\eta \to \infty$, by choosing the proper values of the constants A, B, C_1 and C_2. The perturbed velocity (u', v', w') so obtained is used in equation (47) to give the expression for the actual velocity. The expressions for the velocity are given below:

For parabolic cylinders, the results in terms of $\mathbf{e}_x$ and $\mathbf{e}_z$ unit vectors are

$$\mathbf{u} = U_\infty\left[1 - \frac{\operatorname{erfc}\{\sqrt{(Re/2)}\eta\}}{\operatorname{erfc}\{\sqrt{(Re/2)}\}} - \frac{\eta}{(\xi^2+\eta^2)} \times\left\{\frac{e^{-Re/2} - e^{-Re\eta^2/2}}{\sqrt{(\pi\,Re/2)}\operatorname{erfc}\{\sqrt{(Re/2)}\}}\right\}\right]\mathbf{e}_x + \frac{U_\infty}{(\xi^2+\eta^2)} \times\left[\frac{e^{-Re/2} - e^{-Re\eta^2/2}}{\sqrt{(\pi\,Re/2)}\operatorname{erfc}\{\sqrt{(Re/2)}\}}\right]\mathbf{e}_z. \quad (68)$$

For paraboloids of revolution the velocity vector is

$$\mathbf{u} = U_\infty\left[1-\frac{2}{Re(\xi^2+\eta^2)}\frac{e^{-Re/2}-e^{-Re\eta^2/2}}{E_1(Re/2)}-\frac{E_1(Re\eta^2/2)}{E_1(Re/2)}\right]\mathbf{e}_x + \frac{2U_\infty}{Re}\left[\frac{\xi\sin\phi}{\eta(\xi^2+\eta^2)}\frac{e^{-Re/2}-e^{-Re\eta^2/2}}{E_1(Re/2)}\right]\mathbf{e}_y + \frac{2U_\infty}{Re}\left[\frac{\xi\cos\phi}{\eta(\xi^2+\eta^2)}\frac{e^{-Re/2}-e^{-Re\eta^2/2}}{E_1(Re/2)}\right]\mathbf{e}_z. \quad (69)$$

In equations (68) and (69), the coefficients of $\mathbf{e}_x$, $\mathbf{e}_y$ and $\mathbf{e}_z$ are u, v and w, respectively, and $\mathbf{u} = u\mathbf{e}_x + v\mathbf{e}_y + w\mathbf{e}_z$.

One can use equations (9) and (10) in equation (68) and equations (16)–(18) in equation (69) in order to obtain u for parabolic cylinders and paraboloids of revolution. The expressions so obtained are given below:

For parabolic cylinders the results in terms of $\mathbf{e}_\xi$ and $\mathbf{e}_\eta$ unit vectors are

$$\mathbf{u} = \frac{U_\infty\xi}{\sqrt{(\xi^2+\eta^2)}}\left[1-\frac{\operatorname{erfc}\{\sqrt{(Re/2)}\eta\}}{\operatorname{erfc}\{\sqrt{(Re/2)}\}}\right]\mathbf{e}_\xi - \frac{U_\infty\eta}{\sqrt{(\xi^2+\eta^2)}}\left[1-\frac{\operatorname{erfc}\{\sqrt{(Re/2)}\eta\}}{\operatorname{erfc}\{\sqrt{(Re/2)}\}} - \frac{1}{\eta\sqrt{(\pi\,Re/2)}\operatorname{erfc}\{\sqrt{(Re/2)}\}}\frac{e^{-Re/2}-e^{-Re\eta^2/2}}{}\right]\mathbf{e}_\eta. \quad (70)$$

Consequently

$$u_\xi = \frac{U_\infty\xi}{\sqrt{(\xi^2+\eta^2)}}\left[1-\frac{\operatorname{erfc}\{\sqrt{(Re/2)}\eta\}}{\operatorname{erfc}\{\sqrt{(Re/2)}\}}\right], \quad (71)$$

and

$$u_\eta = -\frac{U_\infty\eta}{\sqrt{(\xi^2+\eta^2)}}\left[1-\frac{\operatorname{erfc}\{\sqrt{(Re/2)}\eta\}}{\operatorname{erfc}\{\sqrt{(Re/2)}\}} - \frac{1}{\eta\sqrt{(\pi\,Re/2)}\operatorname{erfc}\{\sqrt{(Re/2)}\}}\frac{e^{-Re/2}-e^{-Re\eta^2/2}}{}\right]. \quad (72)$$

For paraboloids of revolution

$$\mathbf{u} = \frac{U_\infty\xi}{\sqrt{(\xi^2+\eta^2)}}\left[1-\frac{E_1(Re\eta^2/2)}{E_1(Re/2)}\right]\mathbf{e}_\xi - \frac{U_\infty\eta}{\sqrt{(\xi^2+\eta^2)}}\times\left[1-\frac{E_1(Re\eta^2/2)}{E_1(Re/2)}-\frac{2}{\eta^2\,Re}-\frac{e^{-Re/2}-e^{-Re\eta^2/2}}{E_1(Re/2)}\right]\mathbf{e}_\eta. \quad (73)$$

Therefore

$$u_\xi = \frac{U_\infty\xi}{\sqrt{(\xi^2+\eta^2)}}\left[1-\frac{E_1(Re\eta^2/2)}{E_1(Re/2)}\right], \quad (74)$$

and

$$u_\eta = -\frac{U_\infty\eta}{\sqrt{(\xi^2+\eta^2)}}\times\left[1-\frac{E_1(Re\eta^2/2)}{E_1(Re/2)}-\frac{2}{\eta^2 Re}\frac{e^{-Re/2}-e^{-Re\eta^2/2}}{E_1(Re/2)}\right]. \quad (75)$$

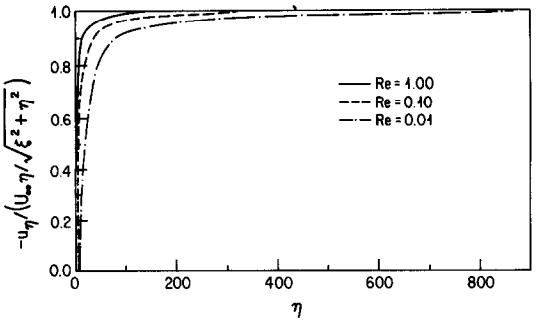

FIG. 3. Velocity profile around parabolic cylinder with OVFA.

In equations (70) and (73), as $\eta\to\infty$, u_ξ and u_η become $U_\infty\xi/\sqrt{(\xi^2+\eta^2)}$ and $-U_\infty\eta/\sqrt{(\xi^2+\eta^2)}$, respectively. These are the components of $\mathbf{U}_\infty$ along the ξ- and η-directions. In the heat transfer analysis it will be seen that only u_η is needed for both parabolic cylinders and paraboloids of revolution. Hence, Figs. 3 and 4 are plotted to show the variation of u_η with respect to η for different values of Re (0.01, 0.1, 1) for the parabolic cylinder and the paraboloid of revolution. In the plot, u_η is normalized with respect to its freestream value, i.e. $-U_\infty\eta/\sqrt{(\xi^2+\eta^2)}$. Both Figs. 3 and 4 show that for low Reynolds numbers the momentum diffuses to a larger distance from the surface of the body, so 'the boundary layer' is thicker. The diffusion of the momentum is larger for parabolic cylinders than it is for the paraboloids of revolution for the same Re. However, for both configurations, the diffusion of momentum extends to distances into the fluid which are much greater than the characteristic dimensions of the body which makes it very tenuous to try to apply boundary layer assumptions.

Substituting equations (71) and (72) in equation (13) and dropping out the Y dependent terms, the energy equation for parabolic cylinders is obtained as

$$\xi\left[1-\frac{\operatorname{erfc}\{\sqrt{(Re/2)}\eta\}}{\operatorname{erfc}\{\sqrt{(Re/2)}\}}\right]\frac{\partial\theta}{\partial\xi} - \eta\left[1-\frac{\operatorname{erfc}\{\sqrt{(Re/2)}\eta\}}{\operatorname{erfc}\{\sqrt{(Re/2)}\}} - \frac{1}{\eta\sqrt{(\pi\,Re/2)}\operatorname{erfc}\{\sqrt{(Re/2)}\}}\frac{e^{-Re/2}-e^{-Re\eta^2/2}}{}\right]\frac{\partial\theta}{\partial\eta} = \frac{1}{Pe}\left[\frac{\partial^2\theta}{\partial\xi^2}+\frac{\partial^2\theta}{\partial\eta^2}\right]. \quad (76)$$

where $\theta = (t-t_\infty)/(t_w-t_\infty)$, and $Pe = U_\infty R/\alpha$. The boundary conditions are:

(1) at $\eta = 1$; $\theta = 1$,

(2) as $\eta\to\infty$; $\theta\to 0$, (77)

(3) at $\xi = 0$; $\dfrac{\partial\theta}{\partial\xi} = 0$,

(4) as $\xi\to\infty$; θ is finite.

Similarly, using equations (74) and (75), in equation (21), and dropping out ϕ dependent terms, the energy

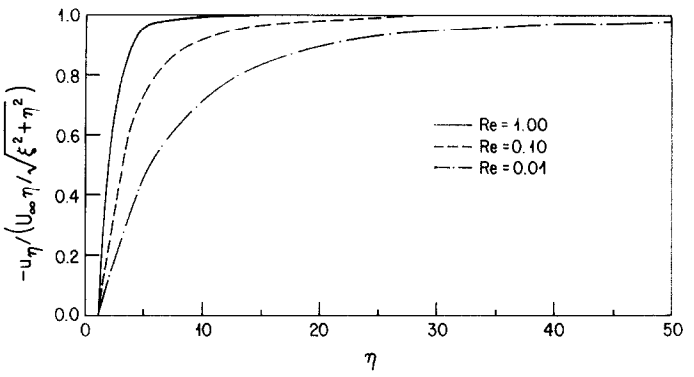

FIG. 4. Velocity profile around paraboloids of revolution with OVFA.

equation for the paraboloid of revolution is obtained as

$$\xi\left[1-\frac{E_1\{Re\,\eta^2/2\}}{E_1\{Re/2\}}\right]\frac{\partial\theta}{\partial\xi}-\eta\left[1-\frac{E_1\{Re\,\eta^2/2\}}{E_1\{Re/2\}}-\frac{2}{Re\,\eta^2}\frac{e^{-Re/2}-e^{-Re\eta^2/2}}{E_1(Re/2)}\right]\frac{\partial\theta}{\partial\eta}=\frac{1}{Pe}\left[\frac{\partial^2\theta}{\partial\xi^2}+\frac{1}{\xi}\frac{\partial\theta}{\partial\xi}+\frac{\partial^2\theta}{\partial\eta^2}+\frac{1}{\eta}\frac{\partial\theta}{\partial\eta}\right]. \quad (78)$$

Equations (77) also represent the boundary conditions for equation (78). The solutions for both parabolic cylinders and paraboloids of revolution are of the same form and can be given as

$$\theta=\frac{t-t_\infty}{t_w-t_\infty}=\frac{\int_\eta^\infty \exp\left[-\int_1^y f(z)\,dz\right]dy}{\int_1^\infty \exp\left[-\int_1^y f(z)\,dz\right]dy}, \quad (79)$$

where

$$f(z)=Pe\,z\left[1-\frac{\operatorname{erfc}\{\sqrt{(Re/2)}z\}}{\operatorname{erfc}\{\sqrt{(Re/2)}\}}-\frac{1}{z\sqrt{(\pi\,Re/2)}}\frac{e^{-Re/2}-e^{-Rez^2/2}}{\operatorname{erfc}\{\sqrt{(Re/2)}\}}\right] \quad (80)$$

(for the parabolic cylinder),

and

$$f(z)=Pe\,z\left[1+\frac{1}{Pe\,z^2}-\frac{E_1(Re\,z^2/2)}{E_1(Re/2)}-\frac{2}{z^2\,Re}\frac{e^{-Re/2}-e^{-Rez^2/2}}{E_1(Re/2)}\right] \quad (81)$$

(for the paraboloid of revolution*).

* For the paraboloid of revolution

$$\int_1^y f(z)\,dz=Pr[1-e^{-Re/2}/E_1(Re/2)]+[1/Pr-2e^{-Re/2}/E_1(Re/2)]\ln y+\frac{Re\,y^2}{2}[1-E_1(Re\,y^2/2)/E_1(Re/2)]+\frac{e^{-Re\,y^2/2}}{E_1(Re/2)}[1-e^{Re\,y^2/2}E_1(Re\,y^2/2)].$$

The temperature profiles, θ vs η, for some selected values of Re (0.1 and 1.0) and Pr (0.01, 1, 10) are plotted in Figs. 5 and 6 for both geometries. One can see that at lower Pr, the temperature profile extends to a larger distance from the body and the 'thermal boundary layer' is thicker. At $Pr = 0.01$, it extends beyond the distance up to which momentum diffuses. One can compare Figs. 3 and 4 with Figs. 5 and 6 to verify this. Under these circumstances boundary-layer assumptions would lead to especially large errors, and misleading results.

The Nusselt number is defined by the heat flux expression given by

$$h(t_w-t_\infty)=-k\left.\frac{\partial t}{\partial n}\right|_{\eta=1}=\frac{-k(t_w-t_\infty)}{R\sqrt{(\xi^2+\eta^2)}}\left.\frac{\partial\theta}{\partial\eta}\right|_{\eta=1}, \quad (82)$$

for both geometries, and using equation (79) in equation (82), one obtains

$$Nu(\xi)=\frac{h(\xi)R}{k}=\frac{1}{\sqrt{(1+\xi^2)}\int_1^\infty \exp\left[-\int_1^y f(z)\,dz\right]dy}, \quad (83)$$

for both parabolic cylinders and paraboloids of revolution. Hence, the Nusselt number at the stagnation point ($\xi = 0$) is given by

$$Nu=\frac{hR}{K}=\frac{1}{\int_1^\infty \exp\left[-\int_1^y f(z)\,dz\right]dy}. \quad (84)$$

Equations (83) and (84), with equation (80), give Nu for the parabolic cylinders, and with equation (81), they give Nu for paraboloids of revolution.

Figures 7 and 8 give the plot of Nusselt number at the stagnation point vs Reynolds number for various Prandtl numbers for parabolic cylinders. Figure 9 gives the same plots for paraboloids of revolution. For both configurations the heat transfer results for high Prandtl number fluids are more sensitive to Reynolds number than for low Prandtl number fluids. Comparing Figs. 7 and 9, one can see how much the shape of the body affects the heat transfer results. Clearly, the Nu are

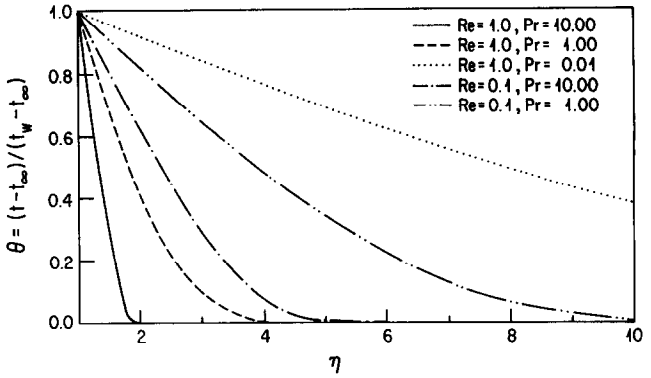

FIG. 5. Temperature profile around parabolic cylinders with OVFA.

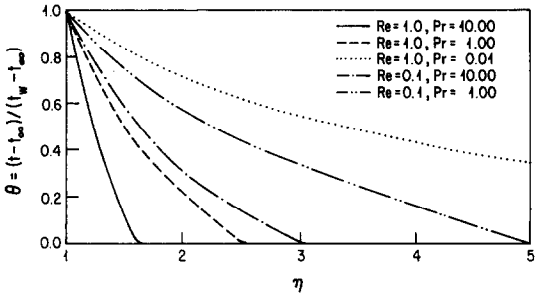

FIG. 6. Temperature profile around paraboloids of revolution with OVFA.

larger for paraboloids of revolution; especially at high *Pr* and low *Re*.

Potential flow approximation

The potential flow velocity u_p for parabolic cylinders is given by Van Dyke [18] and that for paraboloids of revolution is given by Milne-Thomson [19]. In the present work, their potential flow velocity expressions are modified to represent the flow field for the configurations given in Figs. 1(a) and (b). They are

$$\mathbf{u}_p = \frac{U_\infty \xi}{\sqrt{(\xi^2+\eta^2)}}\mathbf{e}_\xi - \frac{U_\infty(\eta-1)}{\sqrt{(\xi^2+\eta^2)}}\mathbf{e}_\eta \qquad (85)$$

(for parabolic cylinders),

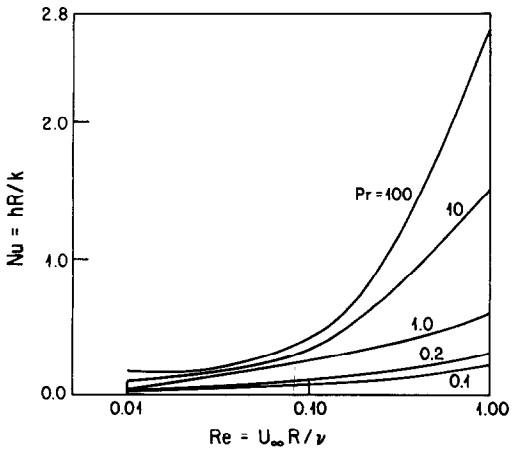

FIG. 7. Nusselt number at the stagnation point vs Reynolds number for parabolic cylinders with OVFA.

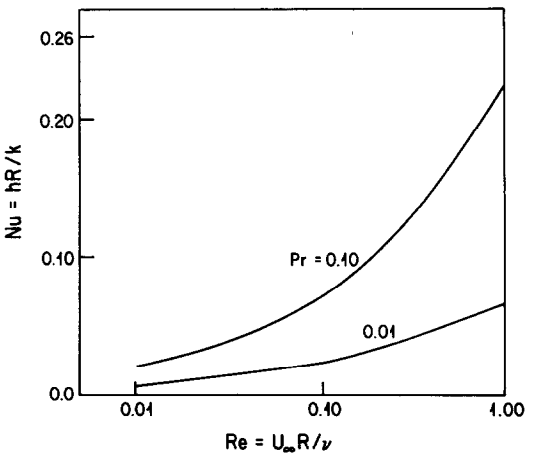

FIG. 8. Nusselt number at the stagnation point vs Reynolds number for parabolic cylinders with OVFA (low Prandtl number results).

and

$$\mathbf{u}_p = \frac{U_\infty \xi}{\sqrt{(\xi^2+\eta^2)}}\mathbf{e}_\xi - \frac{U_\infty(\eta^2-1)}{\eta\sqrt{(\xi^2+\eta^2)}}\mathbf{e}_\eta \qquad (86)$$

(for paraboloids of revolution).

In equations (85) and (86), the coefficient of $\mathbf{e}_\xi$ is $u_{p\xi}$ and that of $\mathbf{e}_\eta$ is $u_{p\eta}$ because $\mathbf{u}_p = u_{p\xi}\,\mathbf{e}_\xi + u_{p\eta}\,\mathbf{e}_\eta$. By

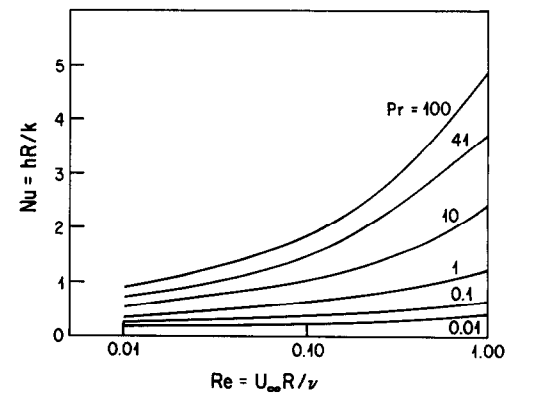

FIG. 9. Nusselt number at the stagnation point vs Reynolds number for paraboloids of revolution with OVFA.

using the values of $u_{p\xi}$, $u_{p\eta}$ from equation (85) in the convection equation for parabolic cylinders, and making the resulting equation dimensionless, one obtains

$$Pe\left[\xi\frac{\partial\theta}{\partial\xi}-(\eta-1)\frac{\partial\theta}{\partial\eta}\right]=\left(\frac{\partial^2\theta}{\partial\xi^2}+\frac{\partial^2\theta}{\partial\eta^2}\right). \quad (87)$$

The dimensionless potential flow convection equation for heat transfer to paraboloids of revolution is given by

$$Pe\left[\xi\frac{\partial\theta}{\partial\xi}-\frac{\eta^2-1}{\eta}\frac{\partial\theta}{\partial\eta}\right]=\left(\frac{\partial^2\theta}{\partial\xi^2}+\frac{1}{\xi}\frac{\partial\theta}{\partial\xi}+\frac{\partial^2\theta}{\partial\eta^2}+\frac{1}{\eta}\frac{\partial\theta}{\partial\eta}\right). \quad (88)$$

The boundary conditions for equations (87) and (88) are the same as equations (77), and the solutions are given below in analytical form

$$\theta=\frac{t-t_\infty}{t_w-t_\infty}=\operatorname{erfc}\left[\sqrt{\left(\frac{Pe}{2}\right)}(\eta-1)\right] \quad (89)$$

(for parabolic cylinders),

$$\theta=\frac{t-t_\infty}{t_w-t_\infty}=\frac{\Gamma(Pe/2,\ Pe\,\eta^2/2)}{\Gamma(Pe/2,\ Pe/2)} \quad (90)$$

(for paraboloids of revolution),

where the incomplete gamma function, $\Gamma(a, x)$ is defined by

$$\Gamma(a,x)=\int_x^\infty e^{-t}t^{a-1}\,dt;\ a>0. \quad (91)$$

Defining the Nusselt number by equation (82) and following the identical procedure used before, one obtains for parabolic cylinders

$$Nu(\xi)=\frac{h(\xi)R}{k}=\frac{1}{\sqrt{(1+\xi^2)}}\sqrt{\left(\frac{2Pe}{\pi}\right)}, \quad (92)$$

which at the stagnation point becomes

$$Nu=\frac{hR}{k}=\sqrt{\left(\frac{2Pe}{\pi}\right)}. \quad (93)$$

For paraboloids of revolution, the Nusselt number is given by

$$Nu(\xi)=\frac{h(\xi)R}{k}=\frac{1}{\sqrt{(1+\xi^2)}}\frac{2(Pe/2)^{Pe/2}\,e^{-Pe/2}}{\Gamma(Pe/2,\ Pe/2)}, \quad (94)$$

which at the stagnation point becomes

$$Nu=\frac{hR}{k}=\frac{2(Pe/2)^{Pe/2}\,e^{-Pe/2}}{\Gamma(Pe/2,\ Pe/2)}. \quad (95)$$

Figure 10 represents the expression for the Nusselt number for both parabolic cylinders and paraboloids of revolution, as given by equations (93) and (95).

Again it is seen that the Nusselt number for paraboloids of revolution is much larger than that for parabolic cylinders, especially at smaller values of Pe.

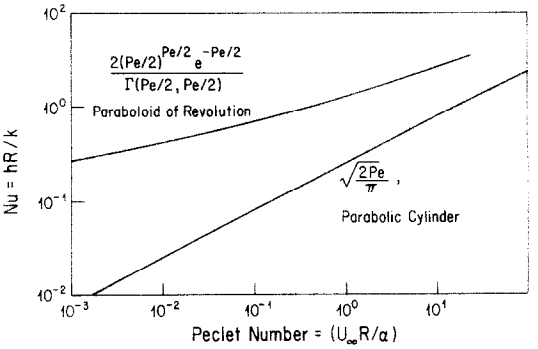

FIG. 10. Nusselt number at the stagnation point vs Peclet number for parabolic cylinders and paraboloids of revolution with the potential flow approximation.

SUMMARY

Analytical solutions have been obtained for convective heat transfer to parabolic cylinders and paraboloids of revolution which should be useful in various applications including developing further our understanding of the effects of convection on dendritic growth. For all flow models studied, heat transfer rates to paraboloids of revolution are substantially higher than to parabolic cylinders, especially at lower values of the Peclet number.

It is noteworthy that the behavior of the heat flux as a function of position along the surface of the isothermal body is consistent with it growing in a shape preserving manner if heat transfer is the controlling mechanism. The results obtained here can be generalized from constant to variable surface temperature bodies by using the Duhamel superposition theorem.

Using the OVFA it is shown that the diffusion of momentum and energy extends to large distances (compared to the tip radius of the body) into the fluid stream, and therefore boundary layer type analyses would be tenuous at best especially for liquid metals. Consequently we have determined solutions for velocity and temperature distributions which do *not* include boundary-layer approximations.

Acknowledgements—This work was supported in part by NSF grant CPE 8112519. Part of the contribution of W. N. Gill was made while on leave as Murphy Distinguished Professor at Iowa State University.

REFERENCES

1. G. P. Ivantsov, *Dokl. Akad. Nauk USSR* **58,** 567 (1947). Translation by G. Horvay in General Electric Report No. 60-RL-2511M (1960).
2. G. Horvay and J. W. Cahn, Dendritic and spheroidal growth, *Acta Metall.* **9,** 695–705 (1961).
3. J. S. Huang, The effect of natural convection in ice crystal growth in salt solution, Ph.D. dissertation, Syracuse University, Syracuse, New York (1975).
4. H. B. Squire, As reported by S. Goldstein, *Modern Developments in Fluid Mechanics*, Vol. 2. Oxford University Press, Cambridge, Massachusetts (1938).
5. N. Frossling, Evaporation, heat transfer and velocity distribution in two-dimensional and rotationally symmetrical laminar boundary layer flow, N.A.C.A. Technical Memorandum 1432 (1958).

6. R. Fernandez and A. J. Barduhn, The growth of ice in flowing water and NaCl solutions, Ph.D. dissertation, Syracuse University, Syracuse, New York, and *Desalination* **3**, 330–342 (1967).
7. J. M. Poisot, The linear growth rate of ice crystals in flowing subcooled water, M.S. thesis, Syracuse University, Syracuse, New York (1968).
8. J. P. Kallungal, The growth of single ice crystal parallel to the A-axis in subcooled quiescent and flowing water, Ph.D. dissertation, Syracuse University, Syracuse, New York (1974).
9. J. P. Kallungal and A. J. Barduhn, Growth rate of ice crystals in subcooled pure water, *A.I.Ch.E. Jl* **23**, 294–303 (1977).
10. J. G. Vlahakis and A. J. Barduhn, Growth rate of an ice crystal in flowing water and salt solutions, *A.I.Ch.E. Jl* **20**, 581–591 (1974).
11. H. C. Simpson, G. C. Beggs, J. Deans and J. Nakamura, The growth of ice crystals, *Desalination* **14**, 341–357 (1974).
12. H. C. Simpson, G. C. Beggs and J. Deans, New theories of the A-axis growth of ice crystals, *Int. J. Heat Mass Transfer* **18**, 615–621 (1975).
13. T. Fujioka, Study of ice growth on slightly undercooled water, Ph.D. dissertation, Carnegie-Mellon University, Pittsburgh, Pennsylvania (1978).
14. J. Cole and A. Roshko, Heat transfer from wires at Reynolds numbers on the Oseen's range, in *Proc. Heat Transfer Fluid Mech. Inst.*, pp. 13–23. University of California, Berkeley, California (1954).
15. C. A. Hieber and B. Gebhart, Low Reynolds number heat transfer from a circular cylinder, *J. Fluid Mech.* **32**, 21–28 (1969).
16. R. T. Davis and M. J. Werle, Numerical solutions for laminar incompressible flow past a paraboloid of revolution, *AIAA J.* **10**, 1224–1230 (1972).
17. J. Wilkinson, A note on the Oseen approximation for paraboloids in a uniform stream parallel to its axis, *Q. J. Mech. Appl. Math.* **8**, 415–421 (1955).
18. M. Van Dyke, Higher approximations in boundary layer theory. Part 3. Parabola in uniform stream, *J. Fluid Mech.* **19**, 145–159 (1964).
19. L. M. Milne-Thomson, *Theoretical Hydrodynamics*. Macmillan, London (1938).

CONVECTION THERMIQUE FORCEE ET TRANSFERT DE QUANTITE DE MOUVEMENT POUR DES STRUCTURES DENDRITIQUES (CYLINDRES PARABOLIQUES ET PARABOLOIDES DE REVOLUTION)

Résumé—Trois modèles théoriques fondamentaux incluant le type d'écoulement rectilinéaire d'Oseen, l'écoulement potentiel et l'approximation du fluide visqueux d'Oseen, sont développés pour le transfert thermique par convection forcée à des cylindres paraboliques et des paraboloïdes de révolution qui représentent une croissance dendritique. Des résultats sont obtenus et présentés en terme de nombre de Nusselt au point d'arrêt lié aux caractéristiques de l'écoulement par des expressions analytiques. Le flux thermique pour les paraboloïdes de révolution est plus important que pour les cylindres paraboliques, particulièrement pour les faibles valeurs du nombre de Péclet. Des expressions locales du flux thermique correspondent à la forme représentant la croissance de ces configurations de dendrites isothermes dans un champ de convection forcée. La diffusion de quantité de mouvement et d'énergie s'étend à des distances nettement plus grandes pour les cylindres paraboliques que pour les paraboloïdes de révolution. Des hypothèses de couche limite conduisent à de fortes erreurs dans les conditions étudiées ici, spécialement pour les fluides à faible *Pr*. Les résultats sont utiles pour décrire aussi la diffusion de masse.

WÄRME- UND IMPULSÜBERGANG AN DENDRITISCHE STRUKTUREN (PARABOLISCHE ZYLINDER UND ROTATIONSPARABOLOIDE)

Zusammenfassung—Es werden drei grundlegende theoretische Strömungsmodelle, nämlich geradlinige Strömung nach Oseen, Potentialströmung und die Approximation für zähe Strömung nach Oseen, entwickelt, um den Wärmeübergang bei erzwungener Konvektion an parabolische Zylinder- und Rotationsparaboloide zu berechnen, welche beim Wachstum von Dendriten eine Rolle spielen. Es werden Lösungen in geschlossener Form erhalten und in Form von Nusselt-Zahlen am Staupunkt dargestellt, die durch analytische Ausdrücke mit Werten in Strömungsrichtung in Beziehung stehen. Der Wärmestrom von Rotationsparaboloiden ist viel größer als der von parabolischen Zylindern, besonders für kleine Werte der Peclet-Zahl. Ausdrücke für den örtlichen Wärmestrom sind konsistent mit dem formerhaltenden Wachstum dieser Konfigurationen von isothermen Dendriten in Feldern mit erzwungener Konvektion. Der Transport von Impuls und Energie erstreckt sich bei parabolischen Zylindern über wesentlich größere Entfernungen in die Strömung als bei Rotationsparaboloiden. Grenzschichtannahmen würden bei den hier untersuchten Bedingungen zu großen Fehlern führen, besonders bei Flüssigkeiten mit niedriger Prandtl-Zahl. Die Ergebnisse eignen sich auch zur Beschreibung des Stofftransports.

ПЕРЕНОС ТЕПЛА И ИМПУЛЬСА ПРИ ВЫНУЖДЕННОЙ КОНВЕКЦИИ К ДЕНДРИТНЫМ СТРУКТУРАМ (ПАРАБОЛИЧЕСКИЕ ЦИЛИНДРЫ И ПАРАБОЛОИДЫ ВРАЩЕНИЯ)

Аннотация—Разработаны три фундаментальные теоретические модели течений, включая модель прямолинейного течения типа озеeновского, модель потенциального течения и модель течения в озеeновском приближении, для исследования теплопереноса вынужденной конвекцией к параболическим цилиндрам и параболоидам вращения, характерным для дендритных образований. Получены решения в замкнутом виде, выраженные через числа Нуссельта для точки торможения, связанные со значениями вниз по потоку с помощью аналитических выражений. Величина теплового потока от параболоидов вращения намного больше, чем от параболических цилиндров, особенно при более низких значениях числа Пекле. Локальные значения теплового потока согласуются с не нарушающим форму образованием этих конфигураций как изотермических дéндритов в поле вынужденной конвекции. Диффузия импульса и энергии распространяется на значительно большие расстояния в поток в случае параболических цилиндров по сравнению с параболоидами вращения. Решения с помощью погранслоя для исследуемых условий могли бы привести к большим ошибкам, особенно в случае жидкостей с малыми значениями числа Прандтля. Результаты могут также использоваться для описания процесса диффузии массы.